Two-dimensional ion-plasma resonances under the surface of liquid helium

Scott Hannahs* and Gary A. Williams
Department of Physics, University of California, Los Angeles, California 90024
(Received 2 April 1990)

The liquid-helium surface is used to confine a two-dimensional plasma of positive helium ions, at a depth under the surface of approximately 300 Å. Plasma-wave resonances are excited and measured over the temperature range from 14 to 400 mK, at ion densities up to $1\times10^8/\text{cm}^2$. The ion effective mass determined from the resonant frequency is measured as a function of temperature, and the limiting $T=0$ value is found to be $m^*=30\pm1$ helium masses. The resonant linewidth measures the ion mobility, which reflects the scattering of the ion from elementary excitations near the helium surface. A change is observed from phonon scattering above 0.2 K to ripplon scattering below that temperature. In the ripplon regime the mobility decreases rapidly as the electric field perpendicular to the surface is increased. The Wigner crystallization transition has been searched for, but no change in the plasma-wave characteristics has been observed over the range $20<\Gamma<2000$, where Γ is the ratio of Coulomb energy to kinetic energy.

I. INTRODUCTION

We report on a series of measurements of the mobility and effective mass of helium ions at the surface of liquid helium. Ions at the surface of liquid helium form a system that has been of considerable experimental and theoretical interest for some time.[1] The ion system is not only a model system for the two-dimensional (2D) Coulomb gas but also allows the measurement of the interaction of electric charges with the helium liquid. These interactions are physically observable as the effective mass and mobility of the ion complexes. These two properties are readily accessible to experimental investigation in this system. The liquid-helium system is also an ideal one in which to investigate the mechanisms for melting in two dimensions.[2] The helium background has a degree of uniformity and purity that cannot be attained for similar systems in semiconductor inversion layers.

The mobility of electrons above the free helium surface was first measured by Sommer and Tanner,[3] which has since led to extensive theoretical and experimental investigations.[4–6] This work reports studies of a system which is similar in many respects, that of positive ions held just below the helium surface. The major differences from the case of electrons in the vapor are the effective mass, which is much greater for ions under the surface, and the presence of direct interactions with the surrounding liquid.

Fluctuations in the ion density obey the two-dimensional Coulomb dispersion relation,

$$\omega^2=\frac{2\pi e^2}{m^*}nk\ , \tag{1}$$

where m^* is the effective mass, k the wave number, and n is the two-dimensional ion density. Appropriate boundary conditions give a resonant standing wave solution. The ion-plasma resonances are used to probe the properties of the two-dimensional ions and their coupling to the helium surface.

The sheet of charge is confined to a circular area by electric fields. Standing wave density oscillations can be driven in a radial breathing mode by a small modulation of the confining electric fields. The first observation of this plasmon mode was made by Ott-Rowland *et al.*[7] for positive ions and later observed by Barenghi *et al.*[8] for electrons under the surface. Similar modes have been observed for electrons above the surface.[9] More recent work on positive ions has been reported by us[10] and by Mellor *et al.*[11,12] The present paper is a more complete description of our results. Section II of this work gives a theoretical overview, Sec. III describes the experimental system and method and, Sec. IV discusses the results and comparisons to theoretical work.

II. THEORY

A. Positive ions in liquid helium

The behavior of ions in helium has been studied by both theorists and experimentalists for nearly 30 years. The original model of the positive ion in helium is due to Atkins.[13] This so-called "snowball model" is due to the solid layer of helium that forms around the ion. The ion has very little zero-point motion due to its high mass, and thus it can be idealized as a point charge. This is in contrast to the less massive electron which forms a bubble, inside of which the electron is in an extended state. A solid layer forms around the positive ion due to the local electrostrictive pressure being larger than the melting pressure of helium. In a simple model[14] the radius R of the snowball is given by

$$\frac{3e^2}{8\pi\epsilon^2R^4}\left[\frac{\epsilon-1}{\epsilon+2}\right]\frac{V_s}{V_l-V_s}\frac{2\sigma_{sl}}{R}+P_\infty=P_m\ , \tag{2}$$

where P_∞ is the ambient pressure of the liquid far from

the ion, P_m is the melting pressure ($\approx$25 bars), ϵ is the dielectric constant of liquid helium (1.0572), V_s and V_l are the molar volumes of liquid and solid He, and σ_{sl} is the solid-liquid surface tension for helium ($\approx$0.135 dyn/cm).[14] If the solid-liquid surface tension is neglected the radius is calculated to be 6.53 Å. An improved model, allowing for the increase in density of the helium at high pressures very near the ion, was calculated by Schwarz.[14]

The total effective mass of the ion is the result of the increased helium density in the neighborhood of the ion, and the hydrodynamic mass of the object. This latter term is due to momentum reversibly transferred to the displaced fluid as the ion complex moves through the superfluid. The surrounding fluid is assumed to be incompressible in this simple model. For a spherical shape this hydrodynamic mass is equal to half the mass of the displaced fluid:

$$M_{\text{hydro}}=\tfrac{2}{3}\pi R^3\rho\ , \tag{3}$$

where ρ is the mass density of the surrounding superfluid. All these factors result in an effective mass on the order of 30–40 helium masses. This mass was measured by the observation of resonant modes in the vertical direction by Poitrenaud and Williams,[15] giving a value of 43.6±2 helium masses and a radius of 6.1 Å at a temperature of 0.7 K. This mass was originally thought to be temperature independent but the work of Ott-Rowland *et al.*[7] and the present results show a significant decrease in the mass at lower temperatures.

B. Confinement of ions at a free surface

The ions in the liquid constitute a single-species plasma. The confinement of this plasma is effected by external electric fields and the free liquid-helium surface. The interaction of the ions with the surface can be modeled as point charges in a simple dielectric material where the ions see an image repulsive force from the surface. An external vertical electric field, denoted $E_\perp$, is also applied to give a stable equilibrium point in the vertical direction (see Fig. 1). The potential as a function of z, the distance from the surface is given by

$$V(z)=\frac{e^2}{4\epsilon}\left[\frac{\epsilon-1}{\epsilon+1}\right]\frac{1}{z}+eE_\perp z\ . \tag{4}$$

The point of stability at which the derivative is zero is given by

$$z_0=\left[\frac{e(\epsilon-1)}{4\epsilon(\epsilon+1)E_\perp}\right]^{1/2}=\frac{3.076\times10^3}{\sqrt{E_\perp}}\ , \tag{5}$$

where for the second expression, if $E_\perp$ is given in volts/cm, z_0 is in Å. For a typical field of 100 V/cm, this gives an equilibrium distance of 308 Å. The small value of the curvature of the well at the minimum gives closely spaced quantum excitation levels. The level spacing of the harmonic-oscillator states is

$$\Delta E=5.22\times10^{-9}E_\perp^{3/2}\text{K} \tag{6}$$

or $\Delta E\approx4.8$ mK for the same typical holding field strength of 100 V/cm. Thus, unlike the system of electrons above the surface, where the electrons sit at the lowest state, the system has several levels populated at even the lowest temperatures reached in this series of experiments ($T=15$ mK) and should be considered as a classical harmonic oscillator in the vertical direction.

In the classical limit we can roughly calculate the fluctuations in the distance to the surface due to thermal excitations in the vertical direction. It can be shown using Eq. (4) that the thickness of the ion sheet increases slowly with the temperature; for typical holding fields of 100 V/cm it increases from a half width of 16 Å at 20 mK to 83 Å at 500 mK. In the limit of assuming a pure harmonic-oscillator potential the width reduces to the calculation of Cole.[6] Even with these fluctuations the system remains two-dimensional because the ratio of the fluctuations to the interparticle spacing ($>1\mu$m) is typically less than 1%.

It has been shown[16] that the activation energy for a current of negative ions through the surface is $\approx$25 K, and that it is not possible for positive ions to penetrate the surface for fields less than 400 V/cm at temperatures less than 1 K. Thus theoretically the system of positive ions can be confined indefinitely; in practice the vibrations of refilling the Dewar with liquid helium cause loss of the confined charge.

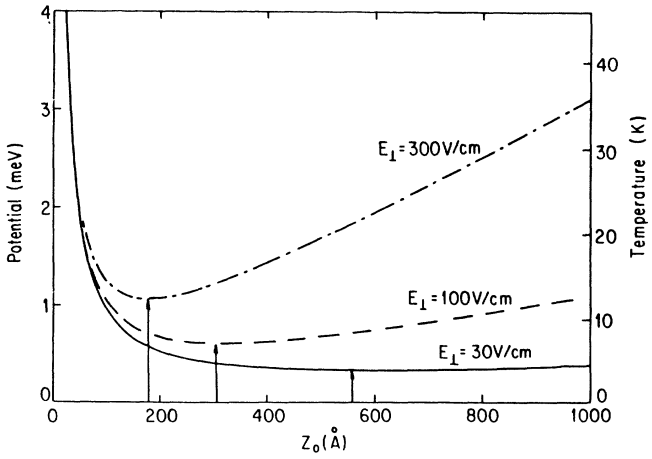

FIG. 1. Potential energy of an ion as a function of the distance from the surface for three different values of the holding field $E_\perp$. The equilibrium points are marked on the axis.

C. Plasma-wave resonance conditions

A schematic of the geometry of the cell is shown in Fig. 2. The solution for the electrical potentials and ion dynamics for this system of charges gives, in the absence of magnetic fields

$$\omega_i^2=\frac{2\pi e^2}{m^*}n_0k_i\mathcal{F}(k_i)\ , \tag{7}$$

where k_i is the set of wave vectors determined by the boundary conditions. The form factor $\mathcal{F}(k)$ is the modification of the ion interaction due to screening of the ions by induced charges on the top and bottom metal plates and to the polarization charge induced by the surface of the helium. The form factor is given by

$$\mathcal{F}(k)=\frac{2\sinh(kd)\sinh[k(h-d)]}{\sinh(kh)\{1+(\epsilon-1)\sinh[k(h-d)]\cosh(kd)/\sinh(kh)\}} . \quad (8)$$

In the limit that $kh\rightarrow\infty$ or the limit where the wavelength is short compared to the spacing between the plates, the form factor reduces to

$$\lim_{k\rightarrow\infty}\mathcal{F}(k)=\frac{2}{1+\epsilon}\lesssim 1 . \quad (9)$$

For the opposite limit where the wavelength is large compared to the spacing the form factor reduces to

$$\lim_{k\rightarrow 0}\mathcal{F}(k)=\frac{2kh(1-d/h)}{1+\epsilon[(1-d/h)/(d/h)]} . \quad (10)$$

Notice that in this limit $\mathcal{F}(k)\propto k$ so that Eq. (7) becomes dispersionless in the low-frequency, long-wavelength limit.

From basic electrostatic theory we know that the potential must vanish at the metallic walls of the cell, $r=R_0$. That is,

$$\phi(R_0)=0 . \quad (11)$$

However, the experimentally observed frequencies match the boundary condition:

$$\left.\frac{d\phi}{dr}\right|_{r=R}=0 , \quad (12)$$

where R is the radius of the charge pool. This is a condition that the ion velocity be zero at the charge pool boundary since $v\propto d\phi/dr$. It was shown by Prasad and Morales[17] that these boundary conditions are consistent and hold at slightly different locations in the cell. The potential is zero at the metallic walls, and the derivative of the potential with respect to r is almost zero at the radius of the charge pool. The radius of the charge pool is not the same as the radius of the cell. Numerical simulations[18,19] show that there is a region of zero charge density between the edge of the charge pool and the edge of the cell. If the dynamical system is modeled, it shows that the slope of the potential is very close to zero at the charge pool radius and the potential itself drops quickly to zero at the cell wall. This is illustrated in Fig. 3 which shows, assuming a step function equilibrium charge density, the variation in potential and the ion velocity as a function of the radius. The equilibrium charge density is shown at the top, with the density dropping to zero at $r=R$. The variation in the density, δn, is shown for the fundamental mode. There is a spike at the edge of the charge sheet where the density changes are due to the expansion of the charge sheet itself under the influence of the driving fields. As can be seen from the figure, the boundary condition that the velocity equal zero at the edge of the charge pool is very close to the actual boundary conditions. Thus the simplified boundary condition $v=0|_{r=R}$ gives quite good agreement with observed frequencies for the dispersion relation. Our results for the first five radial modes are shown in Fig. 4, where the agreement with Eqs. (12) and (7) is better than 3%.

A step function is a reasonable approximation to the actual charge density in the cell. The density actually goes to zero quickly and smoothly. Calculations by Prasad and Morales[17] show that the width of this transition region is entirely determined by the cell geometry. The width of the region δR is given by

$$\delta R=h/\pi , \quad (13)$$

where h is the cell height. For the dimensions used in these series of experiments the fractional width

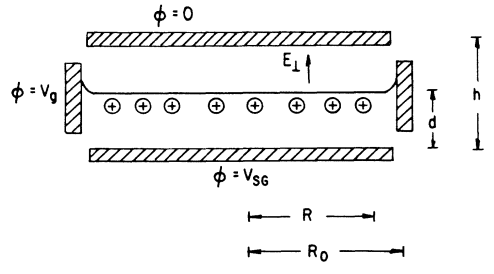

FIG. 2. Schematic of the geometry and variables used to solve the electrodynamics of the experimental cell.

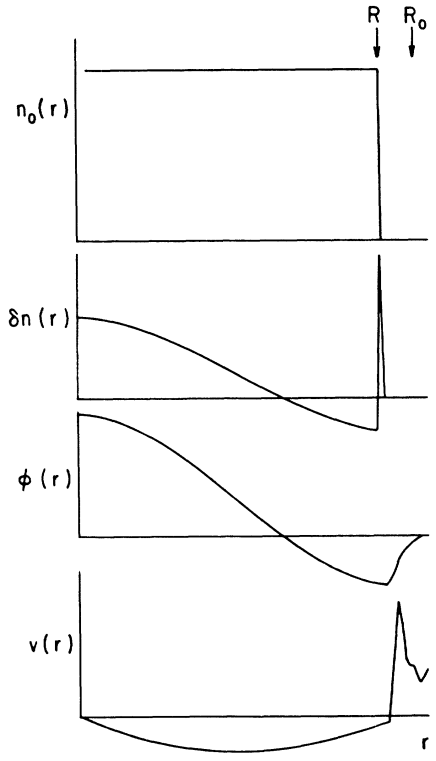

FIG. 3. Calculation by Prasad and Morales for a step function charge density, top; and for the lowest mode, plots of the variation in charge density, the potential and the ion velocity as a function o the radius. The cell edge at R_0 is shown.

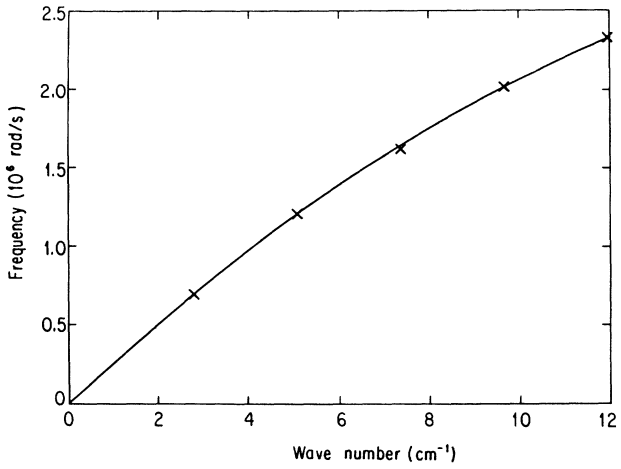

FIG. 4. Resonant frequencies of the five lowest modes of the cell. The solid line is the predicted dispersion.

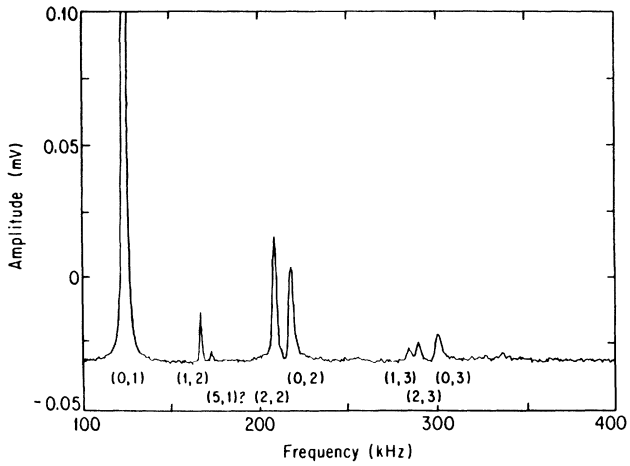

FIG. 5. A response curve showing several azimuthal modes. The modes are labeled (l,n) where l is the azimuthal mode number, and n is the radial mode number. Average of eight sweeps with holding field of 371 V/cm and temperature of 18 mK.

$\delta R/R_0=0.056$, which is a small fraction of the charge pool.

At the edge of the cell where the liquid contacts the walls there is a meniscus, where the liquid surface is curved upwards. Any charges in the region of the meniscus will feel a component of the force normal to the slanted surface in the positive radial direction. This outward force is balanced by the electric field due to the guard ring. Very near the guard ring where the surface is almost vertical, it is not possible to confine the charge and thus there is always a charge depleted region adjacent to the guard ring. For charge densities near the maximum that can be confined by a given set of holding potentials the electrostatic calculation for a flat surface would allow charges in the region near the guard ring. However, the added radial force in the meniscus region causes all charges in the region to flow outward to the confining potential ring and be lost from the system. This effect prevents the cell from being charged to the maximum charge density that is calculated by numerical simulations[17] and care must be taken in changing the confining potential such that charges are not lost from the system.

Though the drive, detection, and boundary conditions are designed to excite only radial modes of the system, azimuthal modes were observed in early experimental runs. Figure 5 shows an example of these modes with identifications of the mode numbers made according to the calculations of Prasad and Morales.[17] The observed modes are a fairly complete set up through the third radial mode and the second azimuthal mode. The frequencies agree well with the numerical predictions and show that the mode structure is well understood. The system may have been sensitive to these nonradial modes due to a slight tilt to the cell. If the axis of the cell is not parallel to the gravitational field, then the liquid surface will not be parallel to the plates generating the holding fields, resulting in a nonuniform charge density. This nonuniform charge density would break the cylindrical symmetry of the system, making it sensitive to azimuthal modes. More careful alignment of the cell in later runs reduced these modes below the noise level.

D. Wigner crystallization

It was first proposed by Wigner[20] that a three-dimensional Fermi system should have an electron-liquid to electron-solid phase transition as the density is lowered. At low enough densities the Coulomb interaction will predominate over the Fermi energy. Subsequently Crandall and Williams[21] showed that a similar transition should occur in a two-dimensional system as the density is increased beyond some critical value. For a two-dimensional system of electrons above the surface of liquid helium, this transition was observed by Grimes and Adams,[9] and later confirmed by shear wave propagation reported by Deville *et al.*[22]

The melting temperature can be expressed in terms of Γ, the ratio of Coulombic to kinetic energy where

$$\Gamma=\frac{e^2\sqrt{\pi n}}{k_B T} \tag{14}$$

and n is the areal density of electrons. Grimes and Adams[23] detected the formation of the crystal by using an rf absorption technique. They observed the crystallization between 0.4 and 0.65 K with densities of $(4–9)\times10^8/cm^2$. They found a critical value of $\Gamma_c=131\pm7$ which agrees well with computer simulations.[24–27] Analytical calculations of the melting transition[28,29] give a phase diagram and mechanism for the solid-liquid transition. Though some numerical simulations show first-order transitions,[30] a number of authors feel that the transition is of the Kosterlitz-Thouless type;[31] in the solid phase the positional order falls off as some power of the distance due to thermally excited dislocation pairs. As the temperature is increased the number of dislocation pairs increases until at a critical temperature the dislocation pairs unbind and the long-

range order falls off exponentially. Thouless[32] applied this model to the two-dimensional electron system and obtained a rough estimate of the critical value $\Gamma_{melt}=78$. These calculations give a transition temperature that is independent of the mass of the ion, and for our system of ions below the surface would predict a similar value of Γ_c as observed for the electron case. The larger mass should not change T_c, and if anything it should make the system even more classical. For our series of experiments, which range in temperature from 13 mK $< T <$ 450 mK with densities of $10^7 < n < 10^8$ cm^2, the values of Γ cover a range of $20 < \Gamma < 2000$. As will be shown later, we have observed no unusual features in the plasma-wave propagation at the transition temperature.

One consequence of the crystallization in this system is the formation of bumps in the helium surface above the localized ions. Ions below the surface of liquid helium can self-trap into states localized in the horizontal plane. The additional energy gained by the regular deformation of the helium surface by charges in a triangular lattice has been calculated by Shikin and Monarkha.[33,34] This binding energy of the ion to the bump is small and if there is no crystallization the localized states will not form at nonzero temperature ($T > 1$ mK). In the crystal state the bumps will form since the binding energy is multiplied by the total number of ions. However, since the effective mass of the bumps is typically only a few electron masses, the bumps have little effect on the positive ions below the surface.

III. EXPERIMENT

A. Experimental apparatus

The experimental cell is similar to that used in previous ion work.[35] The experimental region is contained in a sealed copper cylinder with a cupro-nickel capillary filling tube (0.25 mm i.d.) attached to the side of the cell. All major pieces of the apparatus are constructed of gold plated copper. The cell is mechanically attached to the mixing chamber of a helium dilution refrigerator. A piece of sintered copper of about 0.8 cm^3 is recessed into the inside of the bottom plate for thermal contact to the liquid helium.

The interaction region inside the cell, shown in schematic in Fig. 6, is surrounded by a guard ring of radius 1.53 cm. Small Mylar washers provide electrical isolation from the top plate, above, and the screen grid plate, below. The total height of the interaction region is 0.269 cm. The top plate has a recessed, electrically isolated button of radius 0.51 cm as a capacitive detector. The aperture in the screen grid plate is covered by a mesh screen soldered into a recess. This mesh is composed of gold plated steel wires of 0.028 cm diameter with a center spacing of 0.084 cm.

A field emission technique[36] was used to inject charge into the liquid helium. The field emission tips were electrochemically etched in a solution of potassium hydroxide. This results in tips that were optically sharp when inspected with a 1000× microscope. Several field tips were mounted in parallel below the screen grid so that if one tip degraded due to overheating and melting, the next sharpest tip would automatically replace it. An array of ten tips was normally used thus ensuring that the cell could be used several times without opening and resealing. One set of ten field tips lasted for three separate experimental runs, a total of over 200 chargings of the surface.

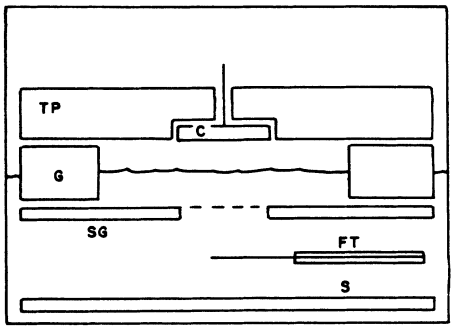

FIG. 6. Schematic of the interaction region of the cell showing the top plate with center button, C; reflector, S; guard ring, G; screen grid, SG; top plate, TP; and the field tips FT (not drawn to scale).

A Speer 100-Ω carbon resistance thermometer sanded flat on one side to expose the resistive element was submerged in the liquid helium below the screen grid. Calibration of this resistor was originally done with a cerium magnesium nitrate thermometer mounted adjacent to it and referenced against an N.B.S. SRM-768 fixed-point temperature standard.[37]

B. Procedure

After the cell was sealed and mounted on the dilution refrigerator it was flushed at least three times with purified helium. The dilution refrigerator was then cooled and the mixture started circulating in the standard manner. After the system reached a base temperature in the millikelvin region, the cell was filled with purified helium to a level of about 40% of the spacing between the screen grid and the top plate by monitoring the capacitance between the center button and the screen grid. At the end of the run the cell was flooded with helium and the filling fraction was once again calculated as a consistency check.

Ordinary helium extracted from natural gas wells contains traces of ^{3}He of a few parts in 10^7. The helium used in this experiment was purified of ^{3}He by flow through a Vycor superleak with a heat flush.[38,39] The method has been known to give a residual ^{3}He concentration of less than one part in 10^{11}, but no attempt was made to measure this for our purification. Levels of one part in 10^{11} for our cell configuration would result in a submonolayer of ^{3}He at the surface with a particle spacing of about 150 Å.

Once the cell was filled and cold, the surface was charged with ions by setting the voltages on the screen

grid and guard ring to the desired values and then applying a voltage to the field tips. A current limiting resistor, about 1.5×10^{10} Ω, was put in series between the high-voltage power supply and the field tips. The voltage on the field tips was increased slowly until a sudden warming of the temperature sensor in the cell was noted. This would occur at a typical voltage of ≈2200 V for reasonably good field tips. This voltage would be applied for 15 to 30 sec and then reduced to 0 V and the field tips connected to electrical ground. It was observed that after charging it would take about 15 to 20 min for the quality factor of a plasma resonance to stabilize. The Q would originally be low, increasing in time to a final steady value. This behavior may be a result of remanent vorticity created by the charging process.

To characterize the system both the frequency and linewidth of the resonant modes were measured. This was done by sweeping slowly and continuously in frequency through the resonance, with the drive on the guard ring generated with a Hewlett Packard 3325A synthesizer/function generator, and simultaneously recording the amplitude of the signal at the center button. The voltage swings on the center button were amplified using an Ithaco 1201 low noise preamplifier and an EG&G 5206 two-phase lock-in analyzer for noise rejection. A schematic of the electronics is shown in Fig. 7.

This amplitude was recorded in real time on a Data Precision D6000 wave-form analyzer and transferred to the laboratory computer for later curve fitting and analysis. Usual sweeps recording 100 points over a range of a few kilohertz were made at a rate of 1 sec per point. Attempts to sweep through a resonance with a higher rate added distortion to the curve and caused an apparent shift in the center frequency. The real time signal from the center button could also be recorded by the waveform analyzer, allowing different frequency components to be measured by a fast Fourier transform technique.

The guard ring and the screen grid were held at fixed voltages by ordinary dc power supplies. A long time constant ($\tau\gtrsim0.5$ sec) filter was attached to the output of the power supplies to prevent small voltage spikes when changing the voltages on the guard ring and screen grid. Such spikes would cause a loss of charge from the surface.

The resonance curve was fitted to a Lorentzian line shape with a linear background. The fitted curve is

$$A(\omega)=\frac{A_0}{[(\omega_0^2-\omega^2)^2+2\omega^2\omega_0^2/(1+2Q^2)]^{1/2}}+b_0+b_1\omega\ , \tag{15}$$

where the amplitude A_0; the center frequency ω_0; the quality factor of the resonance Q; and the linear background b_0 and b_1 can be determined by a least-squares fit to the measured curve. A fit was found using a nonlinear technique due to Levenberg and Marquardt.[40–43] An example of a data sweep and fitted Lorentzian is shown in Fig. 8.

Once the resonance was observed, the temperature or perpendicular electric field was slowly varied and the resonance tracked. The drive level was set at as low a value as possible to still be able to record a clear signal. Even at the lowest drive levels there seemed to be some distortion of the peak from that of a true Lorentzian. However, the drive was below the level where the frequency or quality factor of the peak was a function of drive level.[44] We were unable to determine the causes for this deviation from a true Lorentzian response.

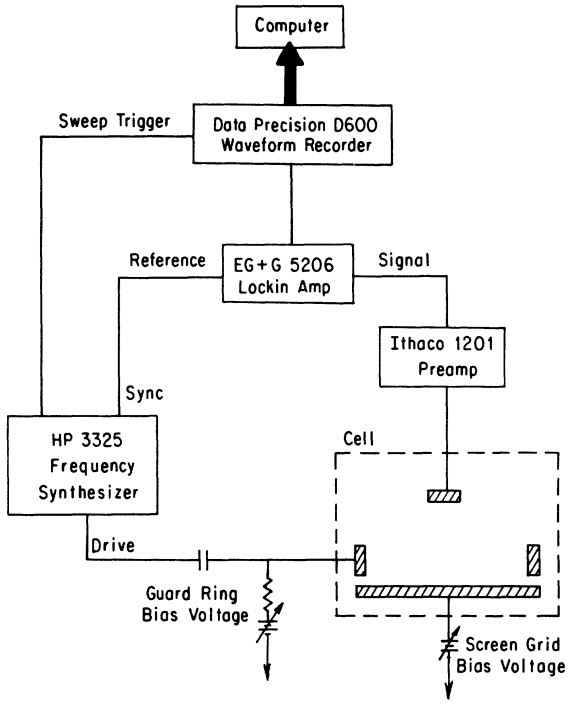

FIG. 7. A schematic of the drive, detection, and recording electronics connected to the cell.

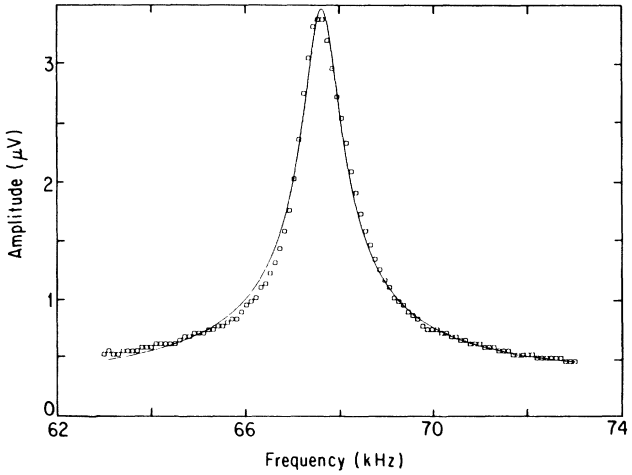

FIG. 8. An example of a recorded frequency sweep with a fitted Lorentzian curve. The data was recorded with $E_\perp=74$ V/cm, $V_g=22.1$ V, with a drive level of 2 mV peak to peak. The fitted parameters are $f_0=67.63$ kHz, $Q=83.57$, and an amplitude of 178.5 μV.

When the perpendicular electric field is changed, the guard-ring voltage must also be changed to keep the charge pool radius constant. To hold this radius constant, the potential difference between the center and the edge of the charge sheet must be held fixed. This condition requires that when the voltage V_{sg} on the screen grid is changed, the voltage V_g on the guard ring must be adjusted such that

$$V_g - V_{sg}(d/h) = \text{const} . \tag{16}$$

That this procedure would hold the charge pool constant (to better than 0.5%) was verified by computer calculations of Prasad.[45] In changing the holding fields the guard ring voltage was always increased first when increasing holding fields to prevent the charge pool from spreading and contacting the guard ring.

It was still noted in initial runs that for some values of the holding fields and densities, the resonant frequency would be a function of the perpendicular electric field. This was usually a reversible dependency in that if the fields were reduced to the original values, the frequency and quality factor would also return to their original values. This implies that charge was not lost from the surface. However, if the perpendicular field was increased beyond a certain value then charge was irreversibly lost from the system. We believe that these anomalous effects result from the charge being forced into the region of the meniscus of the helium surface, where Eq. (16) is not valid. The charge pool radius did not remain constant but expanded, lowering the frequencies and finally resulting in charge loss when the conducting guard ring was contacted. To prevent this from interfering with the measurements, the guard-ring voltage was increased slightly immediately after charging, to compress the charge sheet and keep the edge of the charge pool away from the meniscus region. With this procedure the resonant frequencies remained constant to within 1% when $E_\perp$ was varied.

If the voltage on only the confining guard ring is increased, the charge pool radius will decrease. This will increase both the wave number of the resonance and the density of the ions since the total charge is conserved. Numerical simulations by Prasad[17,45] give the dependence of the charge pool radius on V_g. From the calculated radius the resonant frequency is predicted and shown in Fig. 9. The predicted frequency follows the same form as the measured values, although there is a deviation of about 5% at the highest densities. This agreement with the predicted frequencies shows that the numerical simulations model the charge sheet fairly accurately. The confining fields were at the lowest value when the charge density was measured for this example and thus the effective mass was determined by this point. The density at that point was $3.04\times10^6/\text{cm}^2$, and the effective mass was calculated to be 30.3 helium masses at 14 mK.

C. Charge density measurement

The charge density in the ion sheet was measured at the end of each set of measurements. The method of charge measurement is essentially identical to that used by deGrassie for three-dimensional single-component plasmas.[46] This process releases the charge from the holding fields and thus is a destructive type measurement. The schematic of the electronics setup for this measurement is shown in Fig. 10. The guard ring potential V_g was instantaneously reduced to zero by grounding the connecting lead with a mercury wetted switch while recording the transient exponential decaying voltage on the center button. The relation giving the charge density, taking into account the spacing between the ion layer and the metal plates is

$$n_0 = \frac{\tau \Delta V}{eRAf} , \tag{17}$$

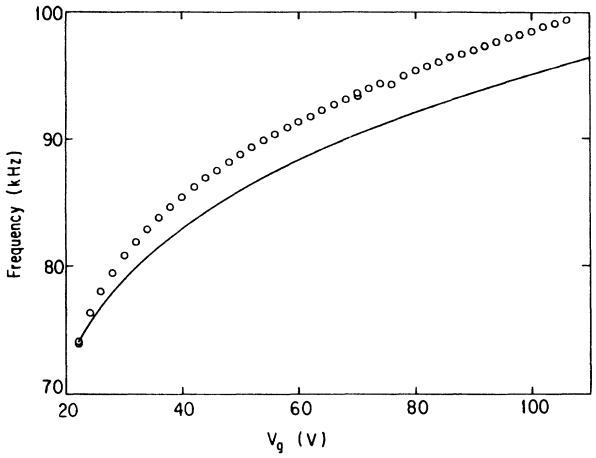

FIG. 9. Resonant plasma frequency as a function of the confining guard-ring voltage. The solid line is the prediction of Prasad (Ref. 45). $T=14.1$ mK, $E_\perp=54.2$ V/cm.

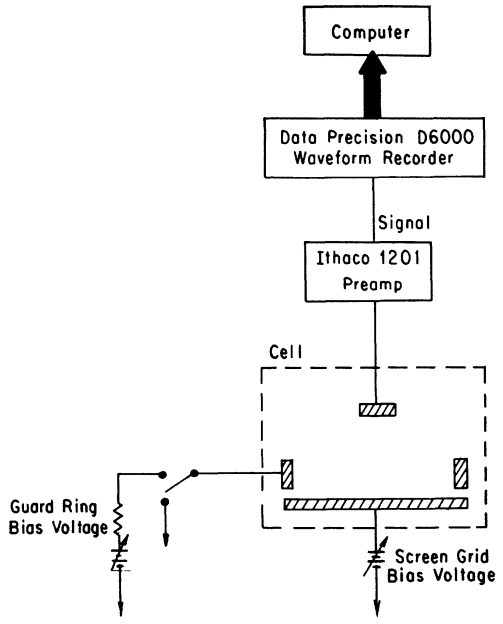

FIG. 10. Schematic of the electronics for measuring the charge density.

where τ is the measured time constant of the decay, ΔV is the voltage jump at the time the guard-ring voltage is turned off, R is the resistance through which the center button discharges (the amplifier input impedance of 10^8 Ω), e is the electronic charge, A is the area of the center button (0.810 cm^2), and $f=d/h$ is the filling fraction (≈ 0.40 in these experiments). A least-squares fit to the form

$$V(t)=\begin{cases}\text{const}, & (t<t_0)\\ \text{const}+\Delta V e^{-t/\tau}, & (t>t_0)\end{cases} \tag{18}$$

is found and the charge density calculated. The region just after t_0 is not weighted as heavily as the rest of the fit since the electronics did not respond fast enough to capture the peak well. The fit to the rest of the decay is quite good as can be seen in Fig. 11 and the value of the jump at $t=t_0$ can be extracted. The background displacement charge induced on the center button by the holding fields for the cell with no trapped ions is also measured and subtracted to determine the actual ion density. This displacement density depended on the magnitude of the holding fields and was $\approx 6\times 10^6/\text{cm}^2$ for $V_{sg}=15$ and $V_g=30$.

Since the area of the center button is well known the uncertainty in measuring the charge density is due to inaccuracy of the fitted parameters. The overall accuracy of the charge density measurement was calculated to be 6%. The charge density was determined after each set of measurements, before the cell was charged to a new density.

IV. RESULTS

A. Ion effective mass

As the temperature of the liquid helium is varied the plasma resonance frequency is found to change. We interpret the changes in frequency as changes in the effective mass of the ion. This phenomenon was originally observed at higher temperatures by Ott-Rowland *et al.*[7] Figure 12 shows that as the temperature increases the resonant frequency decreases substantially. An examination of the dispersion relation,

$$\omega^2=\frac{2\pi e^2}{m^*}n_0\mathcal{F}(k) \tag{19}$$

shows that the only quantity that can possibly be temperature dependent is the effective mass, m^*. If we thus solve for m^* as a function of temperature, all other quantities being known, we get the results shown in Fig. 13. The crosses are derived from the data of Fig. 12 while the circles are based on measurements at a different density and holding field. As can be seen the mass decreases significantly with decreasing temperature. Though the dependence of the effective mass on temperature is well

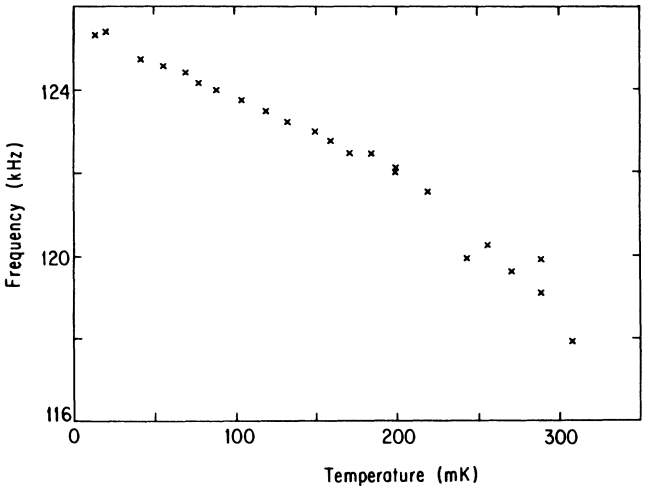

FIG. 12. Frequency of the central resonance peak in kilohertz as a function of temperature.

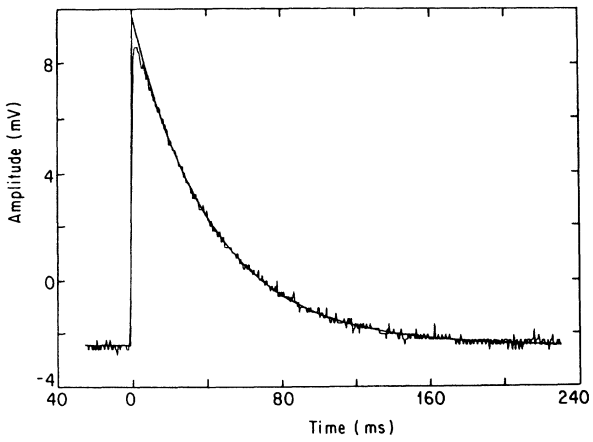

FIG. 11. An example charge dump with fitted exponential decay. $\Delta V=12.23$ mV, $\tau=43.15$ ms giving charge density $n=9.1\times 10^7/\text{cm}^2$.

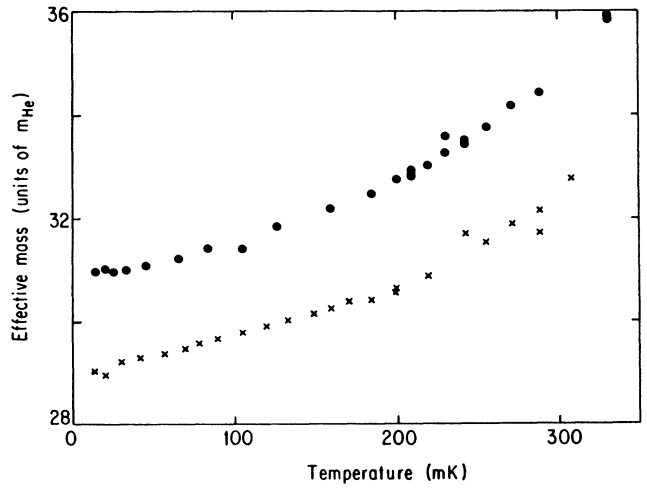

FIG. 13. The ion effective mass in helium masses as a function of temperature; circles, $E_\perp=74$ V/cm, $n=3.2\times 10^7/\text{cm}^2$; crosses, $E_\perp=186$ V/cm, $n=8.92\times 10^7/\text{cm}^2$.

established by the data, the difference between the curves for the two different densities may not be significant since the difference is smaller than the uncertainty in the charge density measurements.

The limiting $T=0$ value of the effective mass can be seen from Fig. 13 to be $30\pm1 M_{\mathrm{He}}$. This is in agreement with the results of Mellor *et al.*[11] who have independently measured the effective mass using similar techniques. Figure 13 shows a lessening of the slope of the effective mass as the temperature is lowered. Earlier work[7] in the higher-temperature regime found a roughly linear behavior with temperature, while the present work demonstrates that the effective mass appears to approach a constant value as $T\rightarrow 0$.

The causes for this temperature dependence of the effective mass are speculative. One possible effect which was considered[7] is an increase in the liquid-solid surface tension with temperature, leading to an increase in the snowball radius and mass. For a 10% increase in the mass of the snowball, the solid-liquid surface tension must decrease also by about 10%. No evidence of temperature dependence of the interfacial tension has been seen,[47–49] though measurements are difficult and possibly dependent on the crystal orientation.[50]

It has been suggested[17,51,52] that the increase in effective mass might be related to the thermal velocity of the ion complex. The hydrodynamic correction to the mass, given by Eq. (3), was derived based on the assumption that the helium liquid is incompressible. If the compressibility of the fluid is accounted for, the hydrodynamic correction becomes a function of the velocity.[51] If the mass is velocity dependent the thermal velocity would also contribute, giving

$$m^*=m_0^*\left[1+\kappa\frac{(v^2+v_t^2)}{c^2}\right], \tag{20}$$

where $v_t^2=3k_BT/m_0^*$ is the ion thermal velocity, v is the velocity due to the electric driving field, and c is the first sound velocity (2.4×10^4 cm/s). The thermal velocity of the ion is about 140 cm/s at a temperature of 10 mK, and the driven ion velocity is of the same order of magnitude when nonlinear effects begin to shift the resonant frequency.[44] Thus the same mechanism which causes the shift in resonant frequency with increasing temperature may also cause the shift in resonant frequency with increasing amplitudes, as is planned to be discussed in a later paper.[53] Such a dependence of the mass on the ion velocity would give a linear temperature dependence to the mass with the intercept at zero temperature a function of the driving amplitude and the "bare" mass. The lower data set in Fig. 13 shows a linear dependence in the low-temperature portion of the plot. A fit of a straight line to this region gives a slope of 8.2 M_{He}/K. This would correspond to a value of $\kappa=75$. The calculation of Putterman *et al.*[51] leads to a value of 0.17 which is a factor of 400 smaller.

A different technique of incorporating the He compressibility was used by Pang,[52] who has considered the emission and absorption of phonons by the ion. The ion-phonon interaction gives rise to an effective mass which increases linearly with T, with a proportionality constant in at least rough agreement with the above results. In the long-wavelength classical limit the result of Pang varies as v_t^2/c^2, in agreement with the result of Putterman *et al.* It is apparently the inclusion of shorter-wavelength phonons which increases the magnitude of the effect.

A different proposal for explaining the effective mass was advanced by Elser and Platzman.[54] They postulated that the microscopic cluster of atoms making up the ion may deviate from spherical symmetry. In motion these misshapen ions would then spin and acquire rotational energy, altering the energy-momentum relationship. Calculations showed that the observed temperature dependence could be accounted for if there was roughly a 30% asymmetry of the ion. This is fairly large, and given the spherical symmetry of the electrostrictive force creating the cluster it is unclear that the weak atom-atom forces could give rise to a modification of the ion shape of that magnitude. That either of these theories[52,54] give a correct quantitative value of the shift in effective mass is unclear at the present time.[55]

B. Mobility

We report measurements of the mobility of the positive ions under the surface by measurement of the plasmon resonance linewidth. These measurements extend down to 14 mK.

The quality factor is proportional to the ion mobility, which is a measure of the scattering of the ion from elementary excitations of the helium. In this experiment these excitations are phonons in the bulk, and ripplons at the helium surface. The mobility is obtained from the quality factor Q by the following relation:

$$\mu=\frac{eQ}{m^*\omega_0}, \tag{21}$$

where ω_0 is the frequency of the resonance.

We have found that the linewidth of the plasma resonance and hence the scattering rate of the ions increases sharply as the temperature is increased. This drop in the quality factor, Q, of the resonance is shown in Fig. 14. The mobility for three different holding fields and densities is shown in Fig. 15. The principal features of the mobility are the constant value up to 150 mK, and the sharp decrease above that temperature. We postulate that the mobility in the low temperature regime is limited by ripplon scattering at the surface, since the phonons are frozen out. At high temperature the mobility decreases as the number of phonons increases rapidly ($n_{\mathrm{phonon}}\propto T^3$).

Our data shows no temperature dependence for $T<100$ mK while that of Mellor *et al.*[12] continues to increase slowly with decreasing temperature. We do not believe that this is due to lack of thermal contact between the ions and the liquid in our experiment since the effective mass remains temperature dependent in this regime. Our results also give a somewhat lower mobility than comparable results of Ref. 12.[56]

The solid line in Fig. 14 shows a T^{-4} dependence and gives a good approximation to the data in the high-

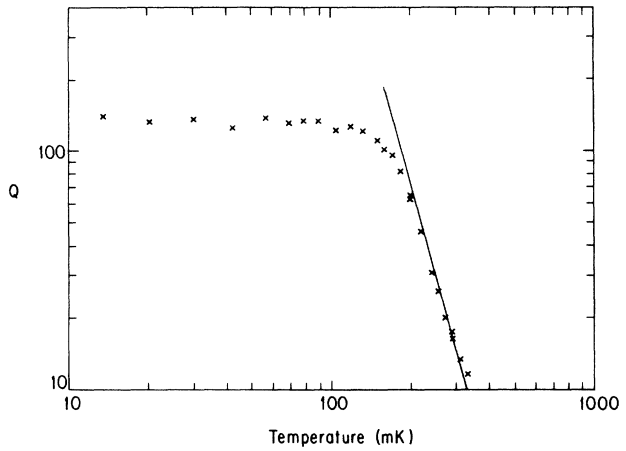

FIG. 14. The quality factor Q, of the resonance as a function of temperature. $n=8.45\times10^7/\text{cm}^2$, $E_\perp=186$ V/cm.

temperature region. A more careful fit to the data in the region of the sharp drop gives a temperature exponent of -5.3 ± 0.4 for the circles in Fig. 14 and an exponent of -3.7 ± 0.4 for the triangles. Schwarz and Stark[57] have calculated the phonon limited mobility for positive ions in bulk superfluid helium. This theory of scattering from ions gives a temperature dependence to the mobility of $\mu\propto T^{-(n+4)}$, where one assumes the scattering cross section $\sigma(k)\propto k^n$. The theory is based on a treatment of the ion moving through a field of thermal excitations being analogous to a particle moving through a gas. At thermal velocities the ion carries about 100 times the momentum of the average phonon so small-angle scattering must dominate. Schwarz measured a temperature dependence approaching T^{-8} for phonon scattering in bulk helium below 0.5 K, in agreement with $n=4$ for Rayleigh scattering.[14] A possible reason for the difference between this result and our observed behavior close to T^{-4} might possibly arise from the ion recoil being mostly limited to the two-dimensional plane, thus changing the allowed phase space of the final state. The characteristics of the phonon and its interaction with the ion may also be modified by the proximity of the surface. In this temperature range the wavelength of a thermally excited phonon is comparable to the distance of the ions from the surface, which may also affect the scattering rate as was suggested by Shikin.[58]

At lower temperatures scattering by phonons becomes less important due to the decreased number of thermally excited phonons. Thus scattering by ripplons becomes the predominant process at the lowest temperatures and limits the mobility in that regime. At these lowest temperatures we find the mobility to be a roughly constant function of temperature, as discussed earlier. In this regime there is a strong dependence of the ion mobility on the holding field $E_\perp$. This effect is shown in Fig. 16 for three different charge densities along with the corresponding derived mobilities. There are two possible explanations for this effect. One is that the matrix element describing the ion-ripplon coupling may be similar to the electron-ripplon case, which is linearly dependent on $E_\perp$. This arises from the interaction energy $eE_\perp\delta z$, where δz is the ripplon oscillation amplitude. The coupling for the electrons above the free surface was first calculated by Shikin and Monarkha[59,60] and later by Platzman and Beni.[61] The mobility for this case is predicted to follow the form

$$\mu=\frac{\mu_0}{(E_0+E_\perp)^2}\ , \tag{22}$$

where $\mu_0=8\sigma\hbar/m^*e$ where σ is the surface tension, and E_0 is linearly dependent on temperature. This temperature dependence of E_0 would predict a weak temperature dependence to the mobility in the ripplon scattering regime.

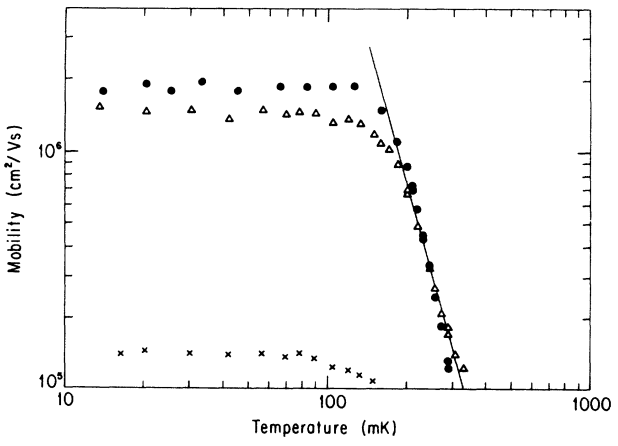

FIG. 15. The mobility as a function of temperature. The solid line is T^{-4} for comparison. Circles: $n=3.2\times10^7/\text{cm}^2$, $E_\perp=74.3$ V/cm; triangles: $n=8.45\times10^7/\text{cm}^2$, $E_\perp=186$ V/cm; crosses: $n=2.56\times10^7/\text{cm}^2$, $E_\perp=372$ V/cm.

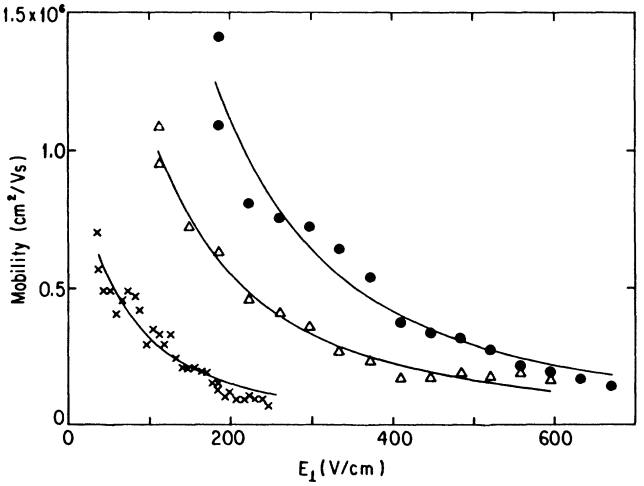

FIG. 16. Derived mobilities as a function of $E_\perp$. The crosses are for $n=6.9\times10^6/\text{cm}^2$; triangles, $n=4.04\times10^7/\text{cm}^2$; circles, $n=8.44\times10^7/\text{cm}^2$. The solid lines are fitted curves as described in the text.

Although the applicability of Eq. (22) can be questioned, we have fit our data to a function of this form. The solid curves in Fig. 16 show the resulting fits. The fitted values of the constants μ_0 and E_0 are summarized in Table I. The value for E_0 is of the same magnitude as the value of 203 V/cm calculated by Platzman and Beni[61] and measured by Grimes and Adams.[9] The fitted value for μ_0 is quite different than the predicted value of $\mu_0 = 9 \times 10^6$ V/s. This large discrepancy in μ_0 may be due to the much larger mass of the positive ions compared with the electron case. Since the momentum of the ion is about 10^5 times larger, small angle scattering dominates and it takes many more scattering events to significantly change the momentum. It is not entirely clear that Eq. (22) can be applied to ions since the derivation assumes electron states above the surface.

Another reason for the dependence of the mobility on $E_\perp$ may be that the ions are being pushed closer to the surface where there may be a direct hydrodynamic interaction. Mellor *et al.*[12] show that interactions of a sphere with surface capillary waves gives rise to a $z_0^{7/2}$ dependence of the mobility. Since $z_0 \propto E_\perp^{-1/2}$ this gives $\mu \propto E_\perp^{-7/4}$ which is difficult to differentiate from the dependence of $\mu \propto E_\perp^{-2}$ predicted by Shikin and Monarkha.[59,60]

Another difference between the electron case and the system studied in these experiments is the occupation of quantum states in the vertical direction. The electrons have been shown by Cole and Cohen[62,63] to occupy only the lowest energy state at the temperatures used in these experiments. In comparison, even below 100 mK, states which extend in the vertical direction are occupied by the positive ions due to the much closer energy spacing. This occupation of the higher states may change the scattering from surface excitations from that of the surface electron case.

Figures 15 and 16 show a density dependence to the mobility of the ions, where increased density of the ions leads to increased mobility. In Fig. 15 the two upper curves have approximately the same mobility even though the perpendicular holding field is much larger for the lower curve. This is due to the greater density of the lower curve which keeps the mobility large. The increase of mobility with density is a puzzling feature, since it is of the opposite sign to that observed for surface electrons.[64]

We have shown that the mobility is limited by phonons at high temperatures and ripplons below 150 mK. In the ripplon-limited regime the variation of the mobility with $E_\perp$ follows the predicted form for electron-ripplon scattering if the magnitude of the scattering term is adjusted. The ion system differs in many important respects from that of the surface electrons, and a more complete theoretical treatment of ion scattering needs to be developed.

TABLE I. The parameters fitted to the values of the mobility, μ using Eq. (22), for three diferent densities.

Density (cm^{-2})	μ_0 (V/s)	E_0 (V/cm)
6.9×10^6	$1.5 \pm 0.1 \times 10^{10}$	120 ± 7
4.0×10^7	$6.6 \pm 0.4 \times 10^{10}$	144 ± 8
8.4×10^7	$1.1 \pm 0.1 \times 10^{11}$	117 ± 17

C. Wigner crystallization

The Wigner crystallization transition has been searched for at all temperatures and ion densities available to this apparatus. As can be seen from Figs. 13 and 14, there is no abrupt feature in either the resonant frequency or the quality factor that would signal the transition. Densities from 5×10^6 to $10^8 cm^2$ have been observed at temperatures from 13 to 450 mK. This results in a range of Γ from 22 to 2200, which should have included the crystallization transition. The factor limiting the range of Γ is that the signal from the lowest charge densities is so poor that the resonance peak cannot be followed to the highest temperatures. The signal would be indistinguishable from the background at about 300 mK for charge densities below $10^7/cm^2$.

Since the experimental parameters have extended so far into the crystal regime, the ions are probably in a crystal lattice. However, the coupling to the plasma wave resonances must be very small to cause no shift in the resonant frequency. The coupling of the plasmon modes of an electron lattice to the ripplon modes has been treated theoretically by Fisher, Halperin, and Platzman[65] and shown to give the modes observed by Grimes and Adams.[9] However, the much larger mass of the positive ions (a factor of 10^5) lowers the frequency of the plasmon mode so much that the lattice Debye frequency (≈ 3 MHz) is comparable to the frequency of a ripplon with a wavelength of the interparticle spacing ($\approx 5-10$ MHz). If lowered enough the coupled modes calculated by Fisher *et al.*[65] would be eliminated. Even though the ripplon frequencies may not intersect the crystal modes, there will still be a small shift in the plasma frequency because the effective mass will include the mass of the "bump" in the helium surface above each ion (if crystallization has occurred). This has been calculated by Fisher *et al.*[65]

$$m^* = m^*_{\text{ion}} + m_{\text{bump}} , \tag{23}$$

where

$$m_{\text{bump}} = \frac{3\rho(eE_\perp)^2}{\sigma^2(8\pi^2/\sqrt{3})^{3/2} n^{1/2}} . \tag{24}$$

For typical values of $E_\perp$ and n this gives effective bump masses on the order of a few electron masses. Since the ion mass is so much larger, the shift of the plasma fre-

TABLE II. Fitted values of negative ion resonances. Frequencies are given in kHz. The holding fields were $E_\perp = -55.8$ V/cm and $V_g = -15$ V.

T (mK)	Resonant frequency (kHz)	Quality factor	Mobility (cm^2/V s)
29.3	51.49	112	3.3×10^5
24.2	21.36	150	1.1×10^6

quency due to this effect would be unobservably small.

Notice that in Fig. 16 there are two different values of the mobility at the lowest holding field. When the data was taken $E_\perp$ was increased until the quality factor had decreased so much as to make the resonance undetectable. The holding field was then reduced to its original value and the resonance was measured again to ensure that the frequency would return to the original value. This was done to ensure that no charge had been lost from the surface during the series of measurements. It was noted that there were sometimes discrepancies in the quality factors (a lower Q) when the fields had been restored to the original values. The origin of this effect is unknown. At this temperature (≈ 15 mK) the ions are most likely in the crystal state and a possibility is that the compression of the charge sheet may cause dislocations to appear in the crystal structure, leading to enhanced dissipation.

D. Negative ions

Negative ions were observed for two separate experimental runs. To charge the surface with negative ions, the cell had to be warmed to about 1 K. At lower temperatures the negative ions would penetrate the surface during the charging process.

After charging the cell was then cooled very slowly to temperatures where the plasmon resonance could be observed. Due to instabilities in ac line voltage or mechanical vibration the charge was unfortunately lost soon after reaching the base temperature. The parameters of the plasma resonance on these two separate runs are summarized in Table II. Due to the inability to keep charge on the surface, no charge density measurements were obtained, and thus no measurement of the effective mass was made. The mobilities given in Table II are derived using an assumed mass of 250 ^{4}He masses. As can be seen from Table II and Fig. 16, the mobilities seem to be comparable to those of the positive ions at these temperatures.

V. CONCLUSIONS

We have measured the effective mass and mobility of positive helium ions held near the free surface of liquid helium. The effective mass is found to be temperature dependent, with a limiting low-temperature value of $m^* = 30 \pm 1 M_{\mathrm{He}}$. Possible explanations of this temperature dependence are proposed, with the most likely to us being the phonon emission models. The ion mobility is measured and seen to have a distinctly different behavior in two regimes. Above 200 mK the mobility is dominated by interaction with phonons with approximately T^{-4} dependence. As the temperature is lowered below 200 mK, the number of phonons decreases and the mobility increases to a limiting value that is determined by the scattering of the ions from ripplons at the helium surface. Our ion mobility in this regime appeared to be independent of temperature. The mobility of the positive ions is seen to be dependent also on the ion density and holding field as well as the temperature. The dependence on the perpendicular electric field is of the form predicted by Shiken and Monarkha, although the overall scale is different. This difference, possibly due to the large mass difference between the electrons and the ions, shows the need for a complete theory of the ion mobility and interaction with the surface.

No indication of Wigner crystallization was seen. Since the experimental parameters are well within the calculated crystal regime as observed for electrons above the surface, it appears that there is very little coupling of the crystal modes to the plasmons. Another method of detecting the regular lattice of the crystal state must be used.

Note added in proof. Mellor and Vinen[66] have now succeeded in observing the crystal transition using an rf technique.

ACKNOWLEDGMENTS

We would like to acknowledge useful discussions with, among others, B. Denardo, A. Larraza, G. Morales, M. L. Ott-Rowland, S. Prasad, S. Putterman, J. Theobald, and W. Vinen. We also thank A. Greenfield for assistance in running the experiment. This work was supported in part by the National Science Foundation, Grant Nos. DMR-84-15705 and DMR 89-12825.

*Present address: Francis Bitter National Magnet Laboratory, MIT, Cambridge, Massachusetts 02139.

[1]T. Ando, A. Fowler, and F. Stern, Rev. Mod. Phys. **54**, 437 (1982).

[2]K. Strandburg, Rev. Mod. Phys. **60**, 161 (1988); **61**, 749(E) (1989).

[3]W. T. Sommer and D. J. Tanner, Phys. Rev. Lett. **27**, 1345 (1971).

[4]V. B. Shikin and Yu. P. Monarkha, Fiz. Nizk. Temp. **1**, 957 (1975) [Sov. J. Low Temp. Phys. **1**, 459 (1975)].

[5]Yu. P. Monarkha and V. B. Shikin, Fiz. Nizk. Temp. **8**, 563 (1982) [Sov. J. Low Temp. Phys. **8**, 279 (1982)].

[6]M. W. Cole, Rev. Mod. Phys. **46**, 451 (1974).

[7]M. Ott-Rowland, V. Kotsubo, J. Theobald, and G. A. Williams, Phys. Rev. Lett. **49**, 1708 (1982).

[8]C. F. Barenghi, C. J. Mellow, C. M. Muirhead, and W. F. Vinen, J. Phys. C **19**, 1135 (1986).

[9]C. C. Grimes and G. Adams, Phys. Rev. Lett. **42**, 795 (1979).

[10]S. Hannahs and G. A. Williams, Jpn. J. Appl. Phys. **26**, Suppl. 26–3, 741 (1987).

[11]C. J. Mellor, C. M. Muirhead, J. Traverse, and W. F. Vinen, Jpn. J. Appl. Phys. **26**, Suppl. 26–3, 381 (1987).

[12]C. J. Mellor, C. M. Muirhead, J. Traverse, and W. F. Vinen, Jpn. J. Appl. Phys. **26**, Suppl. 26–3, 383 (1987).

[13]K. R. Atkins, Phys. Rev. Lett. **116**, 1339 (1959).

[14]K. W. Schwarz, Adv. Chem. Phys. **33**, 1 (1975).

[15]J. Poitrenaud and F. I. B. Williams, Phys. Rev. Lett. **29**, 1230 (1972); **32**, 1213(E) (1974).

[16]L. Bruschi, B. Maraviglia, and F. Moss, in *Proceedings of the Xth International Conference on Low Temperature Physics,*

edited by L. P. Pitaevski and Yu. D. Anufriyev (All Union Institute for Science, Technology, and Information, VINITI, Moscow, 1966), Vol. 1, p. 219.
[17]S. Prasad and G. Morales, Phys. Fluids **30**, 3475 (1987).
[18]R. Mehrota, J. Low Temp. Phys. **123**, 67 (1987).
[19]D. K. Lambert and P. L. Richards, Phys. Rev. B **23**, 3282 (1981).
[20]E. P. Wigner, Phys. Rev. **46**, 1002 (1934).
[21]R. S. Crandall and R. Williams, Phys. Lett. **34A**, 404 (1971).
[22]G. Deville, A. Valdes, E. Y. Andrei, and F. I. B. Williams, Phys. Rev. Lett. **53**, 588 (1984).
[23]C. C. Grimes and G. Adams, Surf. Sci. **98**, 1 (1980).
[24]R. W. Hockney and T. R. Brown, J. Phys. C **8**, 1813 (1975).
[25]R. C. Gann, S. Chakravarty, and G. V. Chester, Phys. Rev. B **20**, 326 (1979).
[26]R. H. Morf, in Proceedings of the Third General Conference of the Condensed Matter Division of the EPS [Helv. Phys. Acta **56**, 743 (1983); Phys. Rev. Lett. **43**, 931 (1979)].
[27]P. Vashishta and R. K. Kalia, in *Proceedings of the Ninth Midwest Solid State Theory Symposium,* edited by R. K. Kalia and P. Vashishta (North-Holland, Amsterdam, 1981), p. 43.
[28]P. M. Platzman and H. Fukuyama, Phys. Rev. B **10**, 3150 (1974).
[29]H. Fukuyama, P. M. Platzman, and P. W. Anderson, Phys. Rev. B **19**, 5211 (1979).
[30]R. K. Kalis, P. Vashista, and S. W. deLeeuw, Phys. Rev. B **23**, 4794 (1981).
[31]J. M. Kosterlitz and D. J. Thouless, J. Phys. C **6**, 1181 (1973).
[32]D. J. Thouless, J. Phys. C **11**, L189 (1978).
[33]Yu. P. Monarkha, Fiz. Nizk. Temp. **1**, 526 (1975) [Sov. J. Low Temp. Phys. **1**, 258 (1975)].
[34]Yu. P. Monarkha and V. B. Shikin, Zh. Eksp. Teor. Fiz. **68**, 1423 (1975) [Sov. Phys.—JETP **41**, 710 (1975)].
[35]J. Theobald, Ph.D. thesis, University of California, Los Angeles, 1984.
[36]A. Hickson and P. V. E. McClintock, in *Proceedings of the 12th International Conference on Low Temperature Physics,* edited by E. Kanda (Academic, Tokyo, 1971), p. 95.
[37]S. R. M. 768 prepared by the Center for Absolute Physical Quantities, National Bureau of Standards, Washington, D. C. 20234.
[38]P. V. E. McClintock, Cryogenics **18**, 201 (1978).
[39]F. E. Moss, A. F. G. Wyatt, and M. J. Baird, Cryogenics **21**, 114 (1981).
[40]D. W. Marquardt, J. Soc. Indust. Appl. Math. **11**, 431 (1963).
[41]K. Levenberg, Quart. App. Math. **2**, 164 (1944).
[42]D. Cline and P. M. S. Lesser, Nucl. Instrum. Methods **82**, 291 (1970).
[43]M. Lampton, B. Margon, and S. Bowyer, Astrophys. J. **208**, 177 (1976).
[44]S. Hannahs, A. Greenfield, and G. A. Williams, Jpn. J. Appl. Phys. **26**, Suppl. 26–3, 753 (1987),
[45]S. A. Prasad (private communication).
[46]J. S. deGrassie, Ph.D. thesis, University of California, San Diego, 1978.
[47]K. O. Keshishev, A. Ya. Parshin, and A. V. Babkin, Pis'ma Zh. Eksp. Teor. Fiz. **30**, 63 (1979) [JETP Lett. **30**, 56 (1979)].
[48]K. O. Keshishev, A. Ya. Parshin, and A. V. Babkin, Zh. Eksp. Teor. Fiz. **80**, 716 (1981) [Sov. Phys.—JETP **53**, 362 (1981)].
[49]S. Balibar, D. O. Edwards, and C. Larouche, Phys. Rev. Lett. **42**, 782 (1979).
[50]S. Balibar and B. Castaing, J. Phys. Lett. **41**, L329 (1980).
[51]S. J. Putterman, P. H. Roberts, and W. Fizdon, Phys. Lett. A **128**, 203 (1988).
[52]T. Pang, Phys. Rev. Lett. **61**, 849 (1988); **61**, 1793(E) (1988).
[53]S. Hannahs, A. Greenfield, B. Denardo, and G. A. Williams (unpublished).
[54]V. Elser and P. M. Platzman, Phys. Rev. Lett. **61**, 177 (1988).
[55]V. Elser and P. Platzman, Phys. Rev. Lett. **64**, 103 (1990); T. Pang, *ibid.* **64**, 104 (1990).
[56]W. F. Vinen (private communication) has indicated they find the mobility in the ripplon regime to be dependent on the cryostat leveling, a factor we did not adjust during the measurements.
[57]K. W. Schwarz and R. W. Stark, Phys. Rev. Lett. **22**, 1278 (1969).
[58]V. B. Shikin, Zh. Eksp. Teor. Fiz. **58**, 1748 (1970) [Sov. Phys.—JETP **31**, 936 (1970)].
[59]V. B. Shikin and Yu. P. Monarkha, J. Low Temp. Phys. **10**, 193 (1974).
[60]V. B. Shikin and Yu. P. Monarkha, Zh. Eksp. Teor. Fiz. **65**, 751 (1973) [Sov. Phys.—JETP **38**, 373 (1973)].
[61]P. Platzman and G. Beni, Phys. Rev. Lett. **36**, 626 (1976); **36** 1350(E) (1976).
[62]M. W. Cole and M. H. Cohen, Phys. Rev. Lett. **23**, 1238 (1969).
[63]M. W. Cole, Phys. Rev. B **2**, 4239 (1970).
[64]R. Mehrota, C. J. Guo, Y. Z. Ruan, D. B. Mast, and A. J. Dahm, Phys. Rev. B **29**, 5239 (1984).
[65]D. S. Fisher, B. I. Halperin, and P. M. Platzman, Phys. Rev. Lett. **42**, 798 (1979).
[66]C. J. Mellor and W. F. Vinen, Surf. Sci. **229**, 368 (1990).